





Cite this: DOI: 10.1039/d5nj02294k

Green synthesis of ZnO-QDs using aqueous *Ficus nitida* leaf extract: phytochemical assessment and biological activity study

Soliman I. El-Hout,^a Marwa H. Suleiman,^{*b} Eslam T. Mohamed,^c
Mohamed A. El Raey,^d Samya El Sherbiny,^b Fatma A. Morsy,^b
Sheta M. Sheta ^{*e} and Said M. El-Sheikh ^{*a}

Quantum dots (QDs) are highly intriguing due to their distinct electronic, optical, and structural characteristics. Most of them still adhere to the old preparation methods that must be extremely precise to achieve this very tiny size of particles. Developing cost-effective, simple, and efficient methods for the preparation of quantum dots would be a breakthrough in nanotechnology. Zinc oxide quantum dots (ZnO-QDs) were successfully prepared employing a green synthesis approach when mediated by aqueous *Ficus nitida* leaf extract. Phytochemical analysis of the *Ficus nitida* leaf extract, including total phenolic content (TPC), total flavonoid content (TFC), DPPH, ABTS, and FRAP assays, showed that the extract contained the necessary phytochemicals and antioxidants for reducing, stabilizing, and capping ZnO-QDs. ZnO-QDs were characterized using XRD, FTIR, SEM, EDX, TEM, XPS, fluorescence spectroscopy, BET and TGA. TEM results showed that the zinc oxide particles formed ranged in size from 2–10 nm. Fluorescence spectra had an emission peak at 423.8 nm confirming the presence of ZnO-QDs at less than 2 nm. The ability to produce quantum dots with biological properties is a significant advantage. The biological activity of the ZnO-QDs against *S. aureus* and *C. albicans* was investigated and validated through molecular docking, yielding auspicious outcomes. Evaluation of the antiviral potential of the ZnO-QDs was conducted through molecular docking analyses against SARS-CoV-2 virus with SARS-CoV-2 RNA polymerase and SARS-CoV-2 spike protein.

Received 2nd June 2025,
Accepted 7th August 2025

DOI: 10.1039/d5nj02294k

rsc.li/njc

Introduction

Quantum dots (QDs), commonly known as “artificial atoms” with a diameter of less than 10 nm, have been central to nanoscience and nanotechnology. QDs exhibit distinctive structural, electrochemical, and photochemical properties, making them an ideal candidate for sensing applications.¹ In recent years, the increasing interest in nanotechnology has resulted in its application across various fields, including engineering,²

physics,³ chemistry,⁴ medicine,⁵ and others. Quantum dots occupy a significant role in nanotechnology since they have distinct structural, electrochemical, and photochemical properties that make them an ideal platform for sensing applications.⁶ Zinc oxide quantum dots (ZnO-QDs) have high exciton binding energy, enabling efficient stimulated emission fluorescence at room temperature. Different sizes of Zn-QDs can generate various fluorescent colors.⁷ ZnO-QDs are not commonly found in nature, are cost-effective to produce, and can be synthesized using established methods.⁸ There is a growing demand for a cost-effective and efficient manufacturing process for producing nanomaterials on a commercial scale giving up on traditional top-down and bottom-up approaches to synthesize nano materials.⁹ The green synthesis approach is a way to avoid the drawbacks of traditional methods for synthesizing quantum dots. It offers non-toxic, eco-friendly, cost-effective, and scalable features.¹⁰ Relying on waste plants, whether industrial, agricultural, or municipal waste, instead of using fresh plants for green synthesis enriches and empowers the concept of sustainability and green synthesis.¹¹ Improper disposal of municipal solid waste can lead to serious environmental and health issues, including infectious diseases,

^a Department of Nanomaterials and Nanotechnology, Central Metallurgical R & D Institute, Cairo 11421, Egypt. E-mail: selsheikh2001@gmail.com; Tel: +20 1022316076

^b Department of Chemistry, Faculty of Science, Helwan University, Cairo 11795, Egypt. E-mail: marwasoliman041@gmail.com; Tel: +20 01095642697

^c Botany and Microbiology Department, Faculty of Science, Helwan University, Ain Helwan, Cairo 11795, Egypt

^d Phytochemistry and Plant Systematics Department, Pharmaceutical and Therapeutic Research Industries Institute, National Research Centre, 12622, Egypt

^e Department of Inorganic Chemistry, National Research Centre, Cairo 12622, Egypt. E-mail: dr.sheta.nrc@gmail.com; Fax: +2-02 33370931; Tel: +20 1009697356

land and water pollution, clogged drains, and loss of biodiversity.¹² *Ficus nitida* is a plant belonging to the *Moraceae* family and is widely cultivated globally. It is a popular street tree in warm climates for its ability to thrive under challenging conditions with minimal requirements. Each year, significant amounts of green *Ficus* leaves are pruned during shaping, leading to environmental concerns due to the accumulation of these leaves.¹³ *Ficus nitida* trees are prevalent throughout Egypt, leading to significant waste from tree trimming.^{14,15} Scientific research revealed that *Ficus* species contain a variety of phytoconstituents such as phenols, flavonoids, alkaloids, tannins, saponins, terpenoids, glycosides, sugars, proteins, essential oils, volatile oils, and steroids, which makes *Ficus nitida* leaves match the requirements of green synthesis using plant extracts.¹⁶ In recent years, the rise in bacterial resistance to antibiotics due to their overuse has posed a significant challenge in healthcare. This necessitates the development of alternative antimicrobial strategies. The antibacterial activities of ZnO QDs against different species of bacteria, fungi and viruses, such as *Escherichia coli*, *Staphylococcus aureus*, *Salmonella pullorum*, and SARS-COV-2, have been reported.^{17–19}

A key challenge in sustainable science is the development of production pathways that are both economically viable and environmentally benign. The core novelty of this work lies in addressing this challenge through the principle of waste valorization. We demonstrate a sustainable and cost-effective approach that transforms discarded municipal green waste into high-value functional nanomaterials.

In this study, an aqueous extract of municipal waste of *Ficus nitida* leaves collected from public gardens at Helwan University campus was prepared. The extract was used as a medium for preparing ZnO quantum dots (QDs). The quantum dots produced are fully characterized, and their antimicrobial activity against *S. aureus* and *C. albicans* and antiviral activity against SARS-COV-2 virus were evaluated.

Results and discussion

The green synthesis method for ZnO-QDs using an aqueous extract of *Ficus nitida* leaves is described in detail in the Experimental section and is represented in Fig. 1.

Phytochemical assessments of AFNLE

Analyzing the phytochemical constituents present in the plant extract would reveal the reason for the formation of nanoparticles mediated by that plant extract. Total phenolic content (TPC), total flavonoid content (TFC), and antioxidant activity represented in DPPH, ABTS, and FRAP techniques of the AFNLE were investigated.

TPC and TFC. The AFNLE had a total phenolic content (TPC) of $103.2 \pm 1.1 \mu\text{g GAE per mg extract}$, expressed as gallic acid equivalent. The total flavonoid content (TFC), expressed as rutin equivalent, was determined to be zero, as shown in Table 1. The presence of phenolics in the AFNLE is responsible



Fig. 1 Scheme of the green synthesis of ZnO-QDs using the aqueous *Ficus nitida* leaf extract.

Table 1 Results of TPC, TFC, DPPH, FRAP, and ABTS analysis of the AFNLE

TPC	TFC	DPPH (IC ₅₀)	DPPH	FRAP	ABTS
μg GAE per mg extract	μg RE per mg extract	μg ml ⁻¹	μM TE per mg sample		
103.2 ± 1.1	Zero	185.6 ± 1	136.3 ± 0.1	525.3 ± 36.9	1870 ± 169.2

for its potent antioxidant activity, essential for nanoparticle formation.

Antioxidant assays of AFNLE. The antioxidant activity of the aqueous *Ficus nitida* leaves extract (AFNLE) was assessed using various methods, including the DPPH assay, presented as IC₅₀ and trolox equivalent (TE) values, as well as the FRAP and ABTS assays. The results of the DPPH assay showed an IC₅₀ value of 185.6 ± 1 μg ml⁻¹ and a trolox equivalent of 136.3 ± 0.1 μM TE per mg extract. In the FRAP assay, the TE was 525.3 ± 36.9 μM TE per mg extract, while in the ABTS assay it was 1870 ± 169.2 μM TE per mg extract. These data are summarized in Table 1. These findings indicate the significant antioxidant potential of the AFNLE, suggesting its possible use in reducing zinc precursor levels.²⁰

Structural and morphological characterization of the ZnO-QDs

XRD analysis. The XRD patterns of the green synthesized ZnO-QDs are illustrated in Fig. 2a. The patterns exhibit diffraction peaks at 2θ values of 31.69°, 34.33°, 36.16°, 47.4°, 56.42°, and 62.67°. These diffraction peaks are coincidental to the (100), (002), (101), (102), (110), and (103) diffraction planes of the hexagonal structure of ZnO, consistent with the standard JCPDS card (No. 01-070-2551). The sharpness and well-defined peaks declare a high degree of crystallinity of the prepared ZnO-QDs. However, as demonstrated in Fig. 2a, a crucial observation is the shift in the peak position of the highest intensity peak (101) at 36.16° in the green-synthesized ZnO-QDs compared to the standard ZnO nanoparticles. This 0.1° shift to a lower 2θ angle suggests the incorporation of phytochemicals from the

AFNLE into the ZnO-QD crystal lattice. These phytochemical constituents likely interact with the ZnO-QDs, causing a slight lattice expansion and, consequently, a shift in the diffraction peak. This confirms the successful integration of AFNLE components within the ZnO-QD structure.

FT-IR spectroscopy. FT-IR analysis is a valuable method to identify the functional groups present in phytochemical constituents capping ZnO-QDs. These functional groups are crucial in reducing, capping, and stabilizing the ZnO-NPs; hence, ZnO-QDs were calcinated at 550 °C to remove all possible functional groups belonging to phytochemicals. Additionally, ZnO-QDs exhibit a characteristic band in the FTIR spectrum. Fig. 2b shows the FTIR spectra of the green synthesized ZnO-QDs recorded within the range of 4000 to 450 cm⁻¹ comparing the produced and calcinated ZnO-QD samples in order to confirm the existence of phytochemical constituents within the produced ZnO-QDs. The prominent broad peak in the higher region at 3382 cm⁻¹ is due to the stretching vibration of hydroxyl (OH) groups, which are associated with phenolic compounds in the AFNLE constituents. The peaks at 2922, 2333, 1570, 1410, 1336, and 1250 cm⁻¹ are assigned to the stretching vibrations of C-H,²¹ C≡N,²² C=O, C-H, C-N, and C-C, respectively, originating from the phytochemicals supported by the AFNLE extract.²³ Finally, the peaks at 830 and 674 cm⁻¹ prove the formation of ZnO-NPs.²⁴ After the calcination of the ZnO-QDs, it is evident that most peaks associated with phytochemical constituents have significantly diminished, with only a few residues of the phytochemicals remaining, resulting in a decrease in the intensity of the peaks.

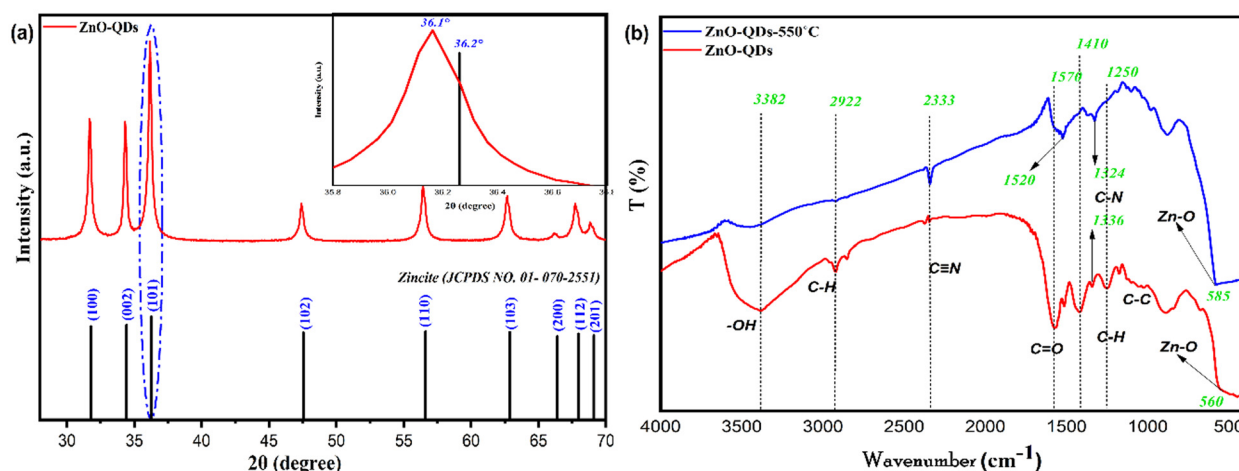


Fig. 2 (a) XRD patterns for ZnO-QDs; the inset is the magnification of the (101) peak, and (b) FT-IR spectra of ZnO-QDs before and after calcination at 550 °C.

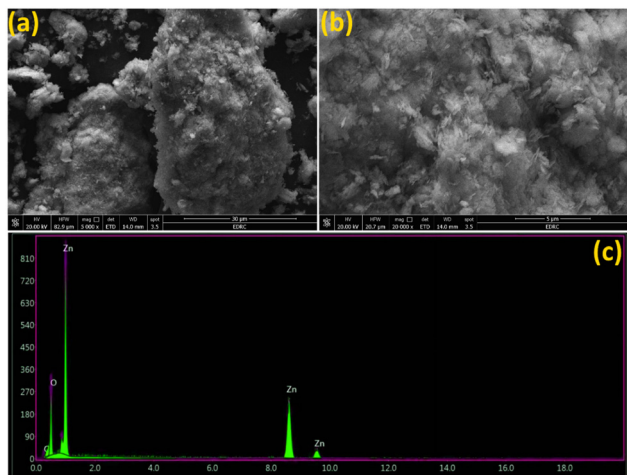


Fig. 3 (a and b) SEM image and (c) EDX of the ZnO-QDs.

Additionally, the peaks at 560 cm^{-1} have shifted to higher wavenumber, specifically 585 cm^{-1} , due to the removal of organic groups causing conjugation.

SEM and EDX analysis. The morphology of the metal oxide quantum dots is a crucial factor determining their surface activity. The green synthesized ZnO-QDs were characterized using scanning electron microscopy (SEM) (Fig. 3), showing particles with a consistent pebble-shaped morphology. This morphology was consistent with the SEM image in Fig. 3a and b, indicating that the AFNLE constituents were sufficient to give the particles their typical shape. An energy dispersive X-ray (EDX) analysis (Fig. 3c) confirmed the presence of Zn and O in the sample, essential for ZnO-QD formation. Additionally, weak peaks of C-atom (carbon) suggested the presence of plant phytochemicals in the sample.

TEM. Fig. 4a and b show the TEM images of the ZnO-QDs synthesized using a green method. The ZnO-QDs have a

pebble-like shape with a hexagonal disk structure for individual particles, indicating a zincite hexagonal crystal structure with diameters ranging from 2 to 10 nm. The TEM images reveal a high level of crystallinity in the nanostructured oxide regions. Light spots in the images represent single nanoparticles, while darker spots indicate aggregation. The presence of phytochemical constituents as capping agents causes the ZnO-QDs to adhere to each other, leading to some aggregation. Fig. 4c displays a selected area electron diffraction (SAED) image of the green-synthesized ZnO-NPs, confirming the crystalline structure of the nanoparticles. The SAED pattern matches the XRD pattern in Fig. 2a, identifying planes (100), (002), and (101) and confirming the presence of ZnO-QDs. The particle size distribution histogram in Fig. 4d provides information on the range of particle size diameters, calculated using ImageJ.

XPS analysis. XPS analysis was carried out to demonstrate the chemical composition of the green synthesized ZnO-QDs. Fig. 5 depicts the survey scan spectrum of the ZnO-QDs, revealing significant peaks at binding energies of 1021 eV (Zn 2p), 530 eV (O 1s), 400 eV (N 1s), and 284 eV (C 1s), confirming the successful synthesis of ZnO-QDs and the presence of phytochemical constituents (Fig. 5a). The high-resolution XPS spectra (Fig. 5b–d) further elucidated the elemental composition and bonding states. In the Zn 2p spectrum (Fig. 5b), the spin-orbit doublet peaks, Zn 2p_{3/2} and Zn 2p_{1/2}, were centered at binding energies of 1022 and 1045 eV, respectively, separated by 23 eV, confirming the successful synthesis of ZnO.²⁵ The O 1s spectrum (Fig. 5c) exhibited three peaks at 531.85, 533, and 533.75 eV corresponding to hydroxyl groups, C–O groups from polyphenols in phytochemical constituents in the AFNLE, and chemisorbed oxygen, which may contribute to the formation of H₂O, CO₂, and/or oxygen defects.²⁶ The C 1s spectrum (Fig. 5d) revealed three peaks at 284.2 eV (C–C),²⁷ 285.56 eV (C–O and/or C–OH),²⁸ and 286.5 eV (C–N),²⁹ further supporting the presence of polyphenolic compounds from the phytochemicals of the AFNLE that acted as capping and stabilizing agents for ZnO-QDs.

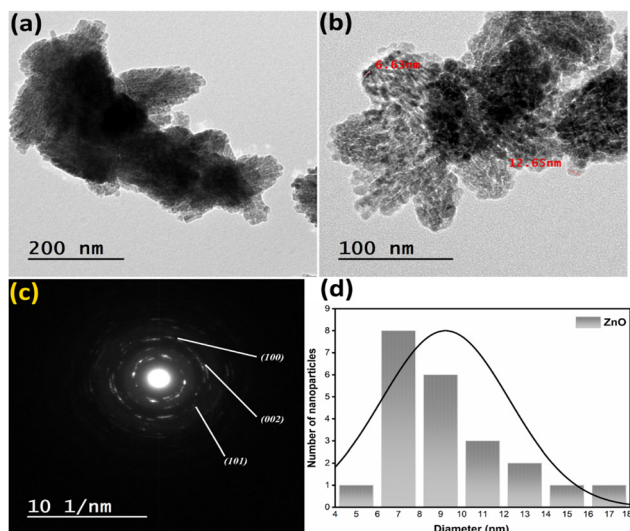


Fig. 4 (a) and (b) TEM images, (c) SAED image, and (d) particle size distribution histogram of the ZnO-QDs.

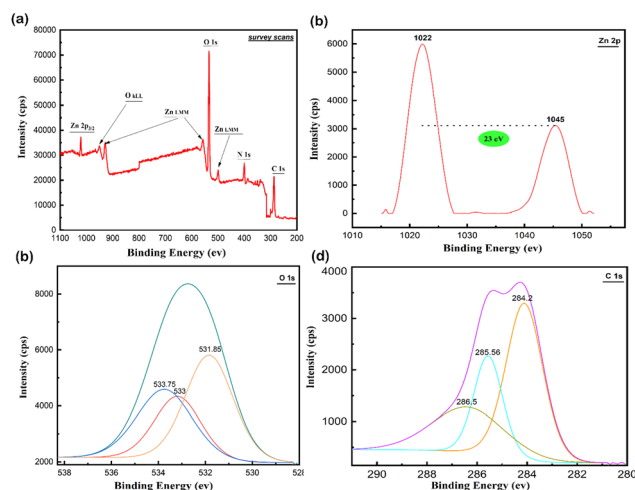


Fig. 5 XPS spectra of the ZnO-QDs: (a) survey scan, (b) Zn 2p, (c) O 1s, and (d) C 1s.

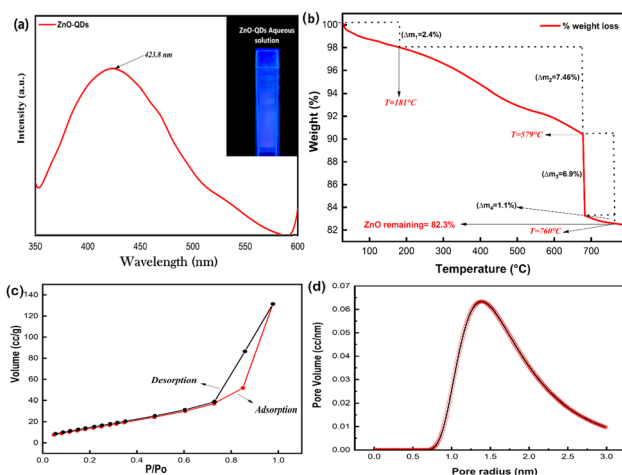


Fig. 6 (a) Fluorescence spectrum of the green synthesized ZnO-QDs; the inset is a photograph of a cuvette with ZnO-QD aqueous solution. (b) Thermogravimetric analysis of the green synthesized ZnO-QDs, (c) BET surface area analysis of the ZnO-QDs, and (d) N_2 adsorption/desorption isotherm.

Fluorescence spectrum. When exposing the ZnO-QD sample to excitation at a wavelength of 365 nm UV light, an emission peak at around 423.8 nm (Fig. 6a) was obtained. This fluorescence emission characteristic of quantum dot particles of ZnO-QDs suggested that the ZnO-QDs particles are less than 2 nm in size.³⁰ Fig. 6a visually demonstrates the fluorescence properties of the ZnO-QD aqueous solution.

TGA analysis. Thermal analysis was performed to study the thermal stability and to determine the yield of the ZnO-QDs. The thermogram (Fig. 6b) reveals that the green synthesized ZnO-QDs underwent three distinct weight loss stages. The first stage (up to 181 °C) exhibited a weight loss of 2.4% due to the evaporation of physically bonded water caused by hydrophilic phytochemicals responsible for water adsorption.³¹ The second stage (up to 579 °C) indicated a weight loss of 7.46%, corresponding to a more significant weight loss, which was likely caused by the decomposition of phytochemical capping agents. The third stage (after 579 °C) involves a sharp weight loss of up to 6.9%, indicating further decomposition of the capping agents. Also, there was a little weight loss of 1.1% in the temperature range (579–760 °C). Primarily, the gradual weight loss is due to the decomposition of phytochemical capping agents of the ZnO QDs. Since these phytochemicals are complex mixtures of organic compounds with varying thermal stabilities, they decompose at various temperatures, leading to a gradual weight loss. After 760 °C, the material remains thermally stable, with no further weight loss. The overall high yield of 82.3% suggests that the proposed synthesis method for ZnO-QDs is effective.

BET analysis. A BET analysis was employed to investigate the surface properties of the synthesized ZnO-QDs, as shown in Fig. 6c. The nitrogen adsorption/desorption isotherm follows (IUPAC) type IV with an H3 hysteresis loop, which indicates a mesoporous structure of the green-synthesized ZnO QDs.³² The BJH pore size distribution curve (Fig. 6d) confirms the presence

of mesopores in the range of 2.8–6 nm.³³ The specific surface area of the ZnO-QDs was calculated to be $60.4 \text{ m}^2 \text{ g}^{-1}$ (BET method) and $107.4 \text{ m}^2 \text{ g}^{-1}$ (Langmuir method).

Biological activity of the ZnO-QDs

Antibacterial and antifungal assessment of the green-synthesized ZnO-QDs. Green-synthesized ZnO-QDs exhibited antimicrobial activity against *S. aureus* ATCC 29213 and *C. albicans* ATCC 10231. The mean inhibition zone diameter for ZnO-QDs was $23.5 \pm 0.5 \text{ mm}$ against *S. aureus* and $22.8 \pm 0.5 \text{ mm}$ against *C. albicans*. The positive control, gentamycin, showed a more significant inhibition zone of $27.2 \pm 0.3 \text{ mm}$ against *S. aureus*. In comparison, clotrimazole had an inhibition zone of $35.2 \pm 0.72 \text{ mm}$ against *C. albicans* (Fig. 7). Statistical analysis revealed that the differences in activity between the ZnO-QDs and the standard controls were highly significant for both *S. aureus* ($p = 0.0018$) and *C. albicans* ($p < 0.0001$). The results demonstrated that the green-synthesized ZnO-QDs possess potent antimicrobial properties against the bacterial (*S. aureus*) and fungal (*C. albicans*) strains. Although the standards were more effective, the strong, statistically significant activity of the ZnO-QDs suggests that the synthesized quantum dots can be a promising alternative to conventional antimicrobial agents. The antimicrobial activity of the ZnO-QDs can be attributed to their unique physicochemical properties, including high surface-to-volume ratio, small size, and ability to generate reactive oxygen species that can disrupt microbial cell membranes and interfere with cellular processes.³⁴ The green synthesis approach using the *Ficus nitida* leaf extract may have also contributed to the enhanced antimicrobial efficacy of the ZnO-QDs by incorporating beneficial phytochemicals from the plant extract.

Ficus nitida, also known as the Indian laurel, is a rich source of various bioactive compounds, including phenolic acids, terpenes, and alkaloids. These phytochemicals possess potent antimicrobial, antioxidant, and anti-inflammatory properties.³⁵ During the green synthesis process, the reducing and capping agents present in the *Ficus nitida* leaf extract may have been incorporated onto the surface of the ZnO-QDs, enhancing their stability and contributing to their antibacterial activity. For instance, flavonoids such as quercetin and kaempferol, commonly

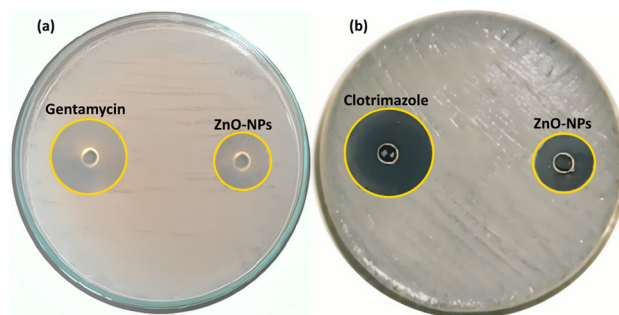


Fig. 7 Agar well diffusion assay plates showing the antimicrobial activity of green-synthesized ZnO-QDs: (a) *S. aureus* ATCC 29213 and (b) *C. albicans* ATCC 10231.

found in *Ficus nitida* leaves, have been reported to disrupt bacterial cell membranes, inhibit enzymes involved in cellular processes, and generate reactive oxygen species that can lead to microbial cell death. Similarly, phenolic compounds like gallic acid and ellagic acid have been shown to interfere with bacterial quorum sensing, protein synthesis, and cell division, thereby inhibiting bacterial growth.³⁶ Furthermore, the synergistic effects between the bioactive components of the *Ficus nitida* leaf extract and the unique properties of the ZnO-QDs may have resulted in the observed enhanced antimicrobial efficacy. The combination of the nanoparticles' ability to generate reactive oxygen species and the antimicrobial properties of the phytochemicals could have contributed to the effective inhibition of both *S. aureus* and *C. albicans*.³⁷

It is important to acknowledge that a direct comparison with the antimicrobial activity of the raw *Ficus nitida* extract was not conducted in this study, as the primary objective was the synthesis, characterization, and confirmation of the inherent biological activity of the ZnO-QDs. The potent activity observed, which is supported by our molecular docking analysis, is attributed primarily to the well-established mechanisms of ZnO nanomaterials. From an economic standpoint, the significance of this work lies in the successful valorization of zero-cost municipal waste into a high-value quantum dot material, a process that opens up applications in biomedicine and sensing far beyond the capabilities of the simple plant extract. Nevertheless, a direct comparative study of the extract *versus* the nanoformulation remains a valuable avenue for future research.

Evaluation of the antibacterial and antifungal potential of ZnO-QDs through molecular docking analyses. The molecular docking analyses revealed the binding interactions between the ZnO-QDs and the target proteins of the selected micro-organisms (Fig. 8a–d). ZnO-QDs were found to bind to the DNA gyrase enzyme (PDB: 6Z1A) with a docking score of $-39.89 \text{ kcal mol}^{-1}$ for *S. aureus*. The quantum dots formed hydrogen bonds with three key residues: Gln 1056(B), Lys 1062(B), and Ser 1063(B). Against *C. albicans*, the ZnO-QDs showed a docking score of $-30.71 \text{ kcal mol}^{-1}$ when interacting with the heat shock protein (Hsp90) (PDB: 6CJL). The quantum dots formed hydrogen bonds with Arg 68(B), Gln 72(B), and Arg 81(B) of the Hsp90 protein. For the SARS-CoV-2 virus, the ZnO-QDs were docked against the RNA-dependent RNA polymerase (RdRp) enzyme (PDB: 7BZF), resulting in a docking score of $-21.61 \text{ kcal mol}^{-1}$. The quantum dots formed hydrogen bonds with Lys 621(A) and Lys 798(A) of the RdRp protein.

The DNA gyrase enzyme in *S. aureus* is responsible for the supercoiling of DNA, which is essential for DNA replication, transcription, and cellular processes. The strong binding affinity of the ZnO-QDs to the DNA gyrase suggests that the quantum dots may disrupt the normal functioning of this enzyme. The formation of hydrogen bonds with key residues could interfere with the DNA gyrase's ability to supercoil the DNA, inhibiting bacterial growth and replication.³⁸ The heat shock protein (Hsp90) in *C. albicans* is crucial in maintaining protein homeostasis and regulating the cellular stress response mechanisms. The formation of hydrogen bonds between ZnO

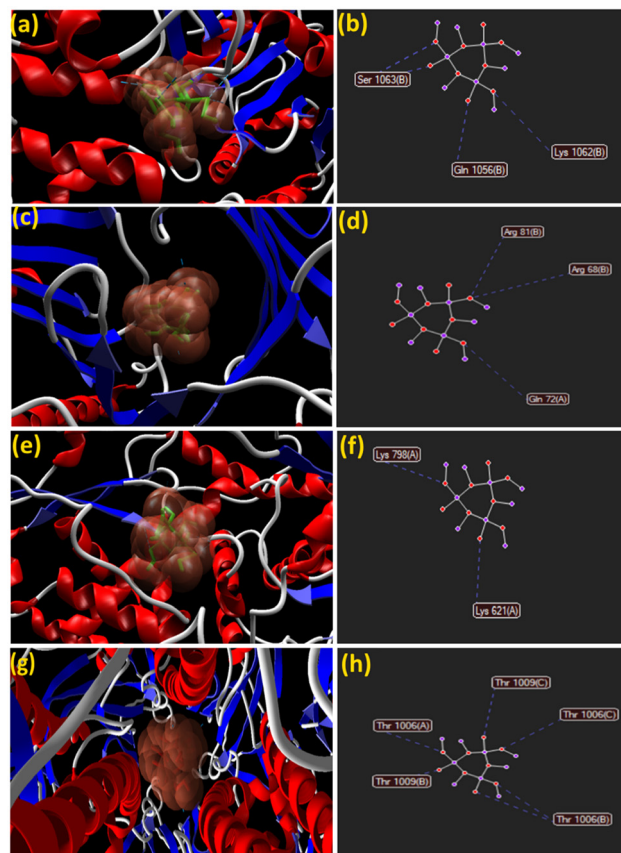


Fig. 8 Binding interactions of ZnO-QDs with: (a) and (b) *S. aureus* DNA gyrase, (c) and (d) *C. albicans* heat shock protein, (e) and (f) SARS-CoV-2 RNA polymerase, and (g) and (h) SARS-CoV-2 spike protein.

quantum dots and Hsp90 suggests that the quantum dots may disrupt the normal folding and functioning of this essential protein. This could impair the fungal pathogen's ability to respond to environmental stresses and maintain cellular integrity, ultimately leading to growth inhibition.³⁹

Evaluation of the antiviral potential of ZnO-QDs through molecular docking analyses against SARS-CoV-2 virus with two different proteins. The RNA-dependent RNA polymerase (RdRp) enzyme in SARS-CoV-2 is responsible for the replication and transcription of the viral genome. As revealed in Fig. 8e–h, the docking of the ZnO-QDs to the RdRp enzyme and the formation of hydrogen bonds indicate that the quantum dots may interfere with the normal enzymatic activity of RdRp. This could potentially disrupt the viral replication process, thereby inhibiting the progression of SARS-CoV-2 infection.^{40,41} Mohammed *et al.* reported the green synthesis of ZnO using an extract of *Cymbopogon citratus* (lemongrass) and evaluated their antibacterial activity against *S. aureus*. Molecular docking studies indicated that the ZnO-QDs could bind favorably to the DNA gyrase subunit B with a binding energy of $-2.93 \text{ kcal mol}^{-1}$. The ZnO-QDs exhibited potent antibacterial activity against *S. aureus*, with a minimum inhibitory concentration of $88.13 \pm 0.35 \mu\text{g ml}^{-1}$.⁴² Nxumalo *et al.* conducted molecular docking studies to investigate the interactions of the green-synthesized

Table 2 Extracts of different plants used for green synthesis of ZnO-QDs and resulting variations in particle shape, size, and antibacterial activity of the quantum dots

Plant	Shape	Particle size (nm)	Antibacterial activity inhibition zone (mm)	
			<i>S. aureus</i>	Ref.
<i>Scoparia dulcis</i>	Pebble-like	20.2	9.5	45
<i>Tetraselmis indica</i>	Spherical	20–40	18.4	46
<i>Cassia fistula</i>	Sponge-like	5–15	10	47
<i>Ficus nitida</i> leaves	Pebble-like structure	2–10	23.47	This work

ZnO-QDs with fungal receptors, comparing them to the standard fungicide propiconazole. The docking results confirmed strong hydrogen-bonding interactions of the ZnO-QDs with fungal receptors in *C. albicans*, suggesting their potential as effective antifungal agents. Hamdi *et al.* performed *in silico* molecular docking studies to investigate the potential antiviral mechanisms of ZnO-QDs against the COVID-19 virus. The docking results showed that the ZnO-QDs could bind to virus receptors, RdRp, and Mpro, potentially inhibiting viral entry, replication, and proliferation. Furthermore, the docking results showed that ZnO-QDs could potentially bind to the SARS-CoV-2 spike protein, which is responsible for the virus's ability to bind to the host cell receptor and initiate the infection process, potentially interfering with viral entry and infection.⁴³ These findings suggest that ZnO-QDs could serve as a promising source for the development of antimicrobial agents. Alam *et al.*,⁴⁴ reported the biogenic synthesis of ZnO-QDs using pine cone extract, which exhibited potent antimicrobial activity against bacteria and fungi. Molecular docking analysis revealed favorable binding interactions between the ZnO-QDs and a bacterial enzyme, suggesting a mechanism for their antimicrobial effects. The biogenic ZnO-QDs were also found to be nontoxic and biocompatible, highlighting their potential for biomedical and environmental applications. Alrabayah *et al.*, synthesized ZnO-QDs using *Cestrum diurnum* L. leaf extract, with an average size of 12.11 nm. The ZnO-QDs showed antiviral activity against the human coronavirus HCoV-229E.⁴⁴

Table 2 compares different plants used for the green synthesis of ZnO-QDs and the resultant shape, size, and antibacterial activity of the nanoparticles. The data revealed that our green synthesized ZnO-QDs have the largest inhibition zone among all materials for the same type of bacteria and the smallest particle size.

Experimental

Materials

5 kg of *Ficus nitida* leaves were brought as waste from public gardens in Helwan University campus, Helwan, Cairo, Egypt. Dehydrated zinc acetate (98% purity) was purchased from El-gomhouria Chemical Company, Cairo, Egypt. Ammonia hydroxide (98% purity) and ethanol (95% purity) were purchased from Merck. All chemicals were used without purification.

Preparation of aqueous *Ficus nitida* leaves (AFNLE)

The *Ficus nitida* leaves were washed with distilled water to remove any dirt or impurities, then dried in the sun for a week.

The dried leaves were ground into small fibers. 100 g of the ground leaves were boiled in 1 l of double-distilled water for 2 hours. The resulting extract was filtered using Whatman no. 1 filter paper to remove plant residues. The filtrate was concentrated into a solid powder using a Heidolph rotary evaporator overnight for any further future yield estimation and storage. Fig. 1 illustrates the process of obtaining the concentrated solid powder of the *Ficus nitida* leaf extract.

Phytochemical assessment of the extract

See more details in the SI.

Green synthesis of ZnO-QDs

The green synthesis method for ZnO-QDs using an aqueous extract of *Ficus nitida* leaves is as follows: 4.0 g of the *Ficus nitida* leaf extract solid powder was dissolved in 1.0 l of double-distilled water. Next, 20.0 g of zinc acetate extract was dissolved in the extract solution. The mixture solution was heated on a direct flame until it reached boiling, maintaining this temperature for about 20 min. A few drops of concentrated ammonium hydroxide were then added until the formation of ZnO-QDs was observed. Following this, the ZnO-QDs were obtained by neutralizing the solution or by heating it until all ammonia is released, leading to the destabilization of the colloidal system. They were then easily collected using the decantation technique, then it was washed several times with double-distilled water and 95% ethanol before being allowed to air-dry for three days, as shown in Fig. 1, the mass of produced ZnO-QDs was about 4 grams. ZnO-QDs are believed to form through the same mechanism proposed by Suleiman *et al.*¹¹

Characterization of ZnO-QDs

See more details in the SI.

Biological activity study for ZnO-QDs

The well diffusion method was used to assess the antimicrobial activity of the ZnO-QDs synthesized from green sources against *Staphylococcus aureus* ATCC 29213 and *Candida albicans* ATCC 10231.⁴⁸ Samples for testing were prepared at a concentration of 30 $\mu\text{g ml}^{-1}$ for the ZnO-QDs, as well as for the positive control antibiotics, gentamycin (30 $\mu\text{g ml}^{-1}$) and antifungal clotrimazole (10 $\mu\text{g ml}^{-1}$). Each test sample (20 μl) was then placed into 5 mm wells on agar plates that had been previously seeded with specific microorganisms. The plates were then incubated at 37 °C for 24 hours for bacteria and at 25 °C for

24 hours for fungi. The diameter of the inhibition zones was measured in millimeters.^{49,50}

Conclusions

ZnO quantum dots (QDs) were successfully synthesized using *Ficus nitida* leaves as a source of municipal waste. The phytochemical analysis of *Ficus nitida* leaves, which included assessing total phenolic content (TPC), total flavonoid content (TFC), and antioxidant assays such as DPPH, ABTS, and FRAP, indicated the presence of essential phytochemicals and antioxidants required for ZnO-QD synthesis. The synthesized ZnO-QDs were thoroughly characterized using various techniques such as XRD, FTIR, TEM, SEM, EDX, XPS, fluorescence spectroscopy, BET, and TGA. TEM analysis revealed a particle size range of 2–10 nm, while fluorescence spectroscopy confirmed the presence of ZnO-QDs with a size below 2 nm. The biological activity of the ZnO-QDs against *S. aureus* and *C. albicans* was evaluated through molecular docking, showing a promising result maximizing the value of waste leaves from the *Ficus nitida* tree.

Conflicts of interest

There are no conflicts to declare.

Data availability

All data generated or analysed during this study are included in this published article and its SI. The SI file included on more details of phytochemical analysis of extract and characterization of ZnO-QDs tools. See DOI: <https://doi.org/10.1039/d5nj02294k>

Notes and references

- M. A. Farzin and H. Abdoos, *Talanta*, 2021, **224**, 121828.
- X. Shen, J. Jia, Y. Lin and X. Zhou, *J. Power Sources*, 2015, **277**, 215–221.
- B. T. Hoan, T. T. Thanh, P. D. Tam, N. N. Trung, S. Cho and V.-H. Pham, *Mater. Sci. Eng. B*, 2019, **251**, 114455.
- H. M. Kashani, T. Madrakian, A. Afkhami, F. Mahjoubi and M. A. Moosavi, *Mater. Sci. Eng. B*, 2019, **251**, 114452.
- A. Arafati, E. Borhani, S. M. S. Nourbakhsh and H. Abdoos, *Ceram. Int.*, 2019, **45**, 12975–12982.
- L. Farzin, M. Shamsipur, L. Samandari and S. Sheibani, *J. Pharm. Biomed. Anal.*, 2018, **161**, 344–376.
- S. Raha and M. Ahmaruzzaman, *Nanoscale Adv.*, 2022, **4**, 1868–1925.
- M. R. Chandana, D. R. Lavanya, B. R. Radha Krushna, B. Daruka Prasad, J. Malleshappa, S. C. Sharma, F. D. Joy, P. Soundararajan and H. Nagabhushana, *Mater. Sci. Semicond. Process.*, 2023, **167**, 107749.
- R. Karmakar, *Prajnan O Sadhona-Sci. Annu.*, 2015, **2**, 116–142.
- Z. Moradialvand, L. Parseghian and H. R. Rajabi, *J. Hazard. Mater. Adv.*, 2025, **18**, 100697.
- M. H. Suleiman, S. M. El-Sheikh, E. T. Mohamed, M. A. El Raey, S. El Sherbiny, F. A. Morsy, S. I. El-Hout and S. M. Sheta, *Dalton Trans.*, 2024, **53**, 18494–18505.
- S. Kumar, M. Adnan, M. Adnan and A. Jha, *Int. J. Adv. Res. Eng. Technol.*, 2020, **11**, 685–693.
- M. M. Emara, R. S. Farag, M. F. Mubarak and S. K. Ali, *Nanotechnol. Environ. Eng.*, 2020, **5**, 1–14.
- H. A. Sorour, *Egypt. J. Plant Prot. Res. Inst.*, 2021, **4**, 57–63.
- A. M. K. A. Aal, O. H. M. Ibrahim, A. Al-Farga and E. A. El Saeidy, *Sustainability*, 2023, **15**, 11762.
- S. Murugesu, J. Selamat and V. Perumal, *Plants*, 2021, **10**, 2749.
- Y. Li, S. Xie, D. Xu, G. Shu and X. Wang, *Nanotechnology*, 2021, **32**, 505104.
- W. A. A. Mohamed, H. H. Abd El-Gawad, S. D. Mekkey, H. R. Galal and A. A. Labib, *Opt. Mater.*, 2021, **118**, 111242.
- J. D. O. Primo, J. D. S. Correa, D. F. L. Horsth, A. Das, M. Zajac, P. Umek, R. Wattiez, F. J. Anaissi, R. C. A. Onderwater and C. Bittencourt, *Nanomaterials*, 2022, **12**, 4345.
- Z. Villagrán, L. M. Anaya-Esparza, C. A. Velázquez-Carriles, J. M. Silva-Jara, J. M. Ruvalcaba-Gómez, E. F. Aurora-Vigo, E. Rodríguez-Lafitte, N. Rodríguez-Barajas, I. Balderas-León and F. Martínez-Esquívias, *Resources*, 2024, **13**, 70.
- M. L. de Peres, R. D. A. Delucis, S. C. Amico and D. A. Gatto, *Nanomater. Nanotechnol.*, 2019, **9**, 1–8.
- Z. Azim, N. B. Singh, S. Khare, A. Singh, N. Amist, Niharika and R. K. Yadav, *Plant Nano Biol.*, 2022, **2**, 100011.
- A. B. Moghaddam, M. Moniri, S. Azizi, R. A. Rahim, A. Bin Ariff, W. Z. Saad, F. Namvar, M. Navaderi and R. Mohamad, *Molecules*, 2017, **22**, 872.
- M. Khan, P. Ware and N. Shimp, *SN Appl. Sci.*, 2021, **3**, 1–17.
- P. Dwivedi, I. Jatrana, A. U. Khan, A. A. Khan, H. Satiya, M. Khan, I. S. Moon and M. Alam, *Nanotechnol. Rev.*, 2021, **10**, 1912–1925.
- E. Zehar, A. Ouerdane, B. Chetti and A. Çoruh, *Mater. Sci. Pol.*, 2023, **41**, 325–338.
- Y. Zhou, S. Liu, Y. Liu, X. Tan, N. Liu and J. Wen, *Int. J. Environ. Res. Public Health*, 2020, **17**, 1–15.
- M. V. Sopinsky, V. S. Khomchenko, V. V. Strelchuk, A. S. Nikolenko, G. P. Olchovyk, V. V. Vishnyak and V. V. Stonis, *Nanoscale Res. Lett.*, 2014, **9**, 1–6.
- C. Battocchio, G. Iucci, M. Dettin, S. Monti, V. Carravetta and G. Polzonetti, *J. Phys.:Conf. Ser.*, 2008, **100**, 052079.
- L. Huang, L. Ding, J. Zhou, S. Chen, F. Chen, C. Zhao, J. Xu, W. Hu, J. Ji, H. Xu and G. L. Liu, *Biosens. Bioelectron.*, 2021, **171**, 112685.
- P. Delmondes and R. Stefani, *MOL2NET*, 2016, **2**, 3862.
- Z. Jowkar, A. Moaddeli, F. Shafiei, T. Tadayon and S. A. Hamidi, *Clin. Exp. Dent. Res.*, 2024, **10**, 1–11.
- S. L. Suib, *Chem. Rec.*, 2017, **17**, 1169–1183.
- I. El-Habib, H. Maatouk, A. Lemarchand, S. Dine, A. Roynette, C. Mielcarek, M. Traoré and R. Azouani, *J. Funct. Biomater.*, 2024, **15**, 195.
- A. D. Adeyemi, C. C. Oluigbo, A. O. Esan, M. O. Bello, S. O. Oladoye, C. P. Emmanuel and E. Effiong, *Biointerface Res. Appl. Chem.*, 2021, **12**, 8003–8034.

- 36 A. Sychrová, G. Škovranová, M. Čulenová and S. Bittner Fialová, *Molecules*, 2022, **27**, 4491.
- 37 A. M. Pillai, V. S. Sivasankarapillai, A. Rahdar, J. Joseph, F. Sadeghfard, K. Rajesh and G. Z. Kyzas, *J. Mol. Struct.*, 2020, **1211**, 128107.
- 38 C. I. Iheme, E. E. Elemike, C. U. Igwe, F. N. Ujowundu, C. U. Ogbonna, Z. C. Uche, O. C. Okoro, I. Hossain and D. C. Onwudiwe, *Inorg. Chem. Commun.*, 2024, **160**, 111864.
- 39 Y. N. Slavin and H. Bach, *Nanomaterials*, 2022, **12**, 4470.
- 40 S. R. Kurnianto, A. G. B. Simarmata, J. F. Fatriansyah, M. Anis, R. K. Rizqillah and M. A. Yasin, in *AIP Conference Proceedings*, AIP Publishing, 2024, vol. 3080.
- 41 I. N. Alrabayah, S. S. Elhawary, Z. A. Kandil, E. M. A. El-Kadder, Y. S. Moemen, A. M. Saleh and M. A. El Raey, *Molecules*, 2022, **28**, 266.
- 42 K. A. Nxumalo, J. O. Adeyemi, T. B. Leta, T. M. Pfukwa, S. N. Okafor and O. A. Fawole, *Sci. Rep.*, 2024, **14**, 18071.
- 43 M. Hamdi, H. M. Abdel-Bar, E. Elmowafy, A. El-Khouly, M. Mansour and G. A. S. Awad, *ACS Omega*, 2021, **6**, 6848–6860.
- 44 M. Alam, *Nanotechnol. Rev.*, 2021, **10**, 1079–1091.
- 45 V. S. Sivasankarapillai, N. Krishnamoorthy, G. E. Eldesoky, S. M. Wabaidur, M. A. Islam, R. Dhanusuraman and V. K. Ponnusamy, *Appl. Nanosci.*, 2023, **13**, 6093–6103.
- 46 G. S. Thirumoorthy, O. Balasubramaniam, P. Kumaresan, P. Muthusamy and K. Subramani, *Bionanoscience*, 2021, **11**, 172–181.
- 47 D. Suresh, P. C. Nethravathi, Udayabhanu, H. Rajanaika, H. Nagabhushana and S. C. Sharma, *Mater. Sci. Semicond. Process.*, 2015, **31**, 446–454.
- 48 Z. Obeizi, H. Benbouzid, S. Ouchenane, D. Yilmaz, M. Culha and M. Bououdina, *Mater. Today Commun.*, 2020, **25**, 101553.
- 49 A. D. Adeyemi, C. C. Oluigbo, A. O. Esan, M. O. Bello, S. O. Oladoye, C. P. Emmanuel and E. Effiong, *Biointerface Res. Appl. Chem.*, 2022, **12**, 8003–8034.
- 50 A. S. Bhosale, K. K. Abitkar, P. S. Sadalage, K. D. Pawar and K. M. Garadkar, *J. Mater. Sci.: Mater. Electron.*, 2021, **32**, 20510–20524.